Disrupting Helix Formation in Unsolvated Peptides

David T. Kaleta and Martin F. Jarrold*

Department of Chemistry, Northwestern University, 2145 Sheridan Road, Evanston, Illinois 60208

Received: December 11, 2000; In Final Form: February 22, 2001

Protonated polyalanine peptides form helices in the gas phase when their most basic protonation site (the N-terminus) is blocked by acetylation: Ac-A_n+H^+ (Ac = acetyl and A = alanine). The glycine analogues, Ac-G_n+H^+ (*G* = glycine), on the other hand, form random globules. The disruption of helix formation in unsolvated Ac-$A_nG_xA_m$+H^+ peptides has been examined as a function of $n+m$, and x using high resolution ion mobility measurements and molecular dynamics simulations. A surprisingly large block of glycine residues is required to disrupt helix formation in these peptides. For example, Ac-$A_5G_3A_5$+H^+ and Ac-$A_6G_5A_6$+H^+ both remain helical at room temperature. According to molecular dynamics simulations, the glycines do not cause a localized disruption of the helices, as might be expected for a residue considered a helix breaker. This is consistent with helix disruption occurring through a global effect on the relative energies of the helix and globule rather than through a localized entropic effect.

Introduction

The question of why particular amino acids tend to form secondary structure strikes at the heart of the protein folding problem. The aggregation of secondary structures leads to the native conformation of a protein, which ultimately determines functionality. In solution, the native conformation is determined by a complex mixture of intramolecular forces and hydration interactions. Recently, there has been growing interest in examining topics such as secondary structure formation in the gas phase.[1] If we can obtain a thorough understanding of the basic issues such as helix formation in unsolvated peptides, we will be in a much better position to understand these processes throughout the range of biologically relevant environments, from aqueous solution to the interior of membranes.

Of the naturally occurring amino acids, alanine has the highest propensity to form helices in aqueous solution, whereas glycine exhibits one of the lowest.[2−6] However, protonated polyalanine and polyglycine peptides both form globules (compact, roughly spherical conformations) in the gas phase.[7] The protonated polyalanine peptides fail to adopt a helical conformation because of the location of the charge. The most basic protonation site is at the N-terminus.[8] However, the N-terminus is also the positive end of the helix macrodipole,[9] and so protonation at the N-terminus destabilizes the helix. Protonation at the C-terminus, on the other hand, stabilizes the helical conformation. With the N-terminus blocked by acetylation and with a lysine at the C-terminus to locate the charge, a helical conformation results for polyalanine-based peptides, Ac-A_nK+H^+ (Ac=acetyl, A = alanine, and K = lysine),[10] but not for their glycine analogues, Ac-G_nK+H^+ (G = glycine).[11] For the polyalanine-based peptides it is possible to switch the helix on and off by moving the lysine from the C-terminus (helix) to the N-terminus (globule).

In this article we describe studies of helix disruption caused by inserting a block of glycine residues into a polyalanine peptide, Ac-$A_nG_xA_m$+H^+. On the basis of what is known about helix formation in solution,[2,6] we anticipate that relatively few glycines will disrupt helix formation in vacuo. The conformations of the unsolvated peptides were probed using high-resolution ion mobility measurements.[12] It has previously been shown that this approach can distinguish between helices and globules for unsolvated peptides.[13] Molecular dynamics (MD) simulations were performed for the 15-residue forms of the Ac-$A_nG_xA_m$+H^+ peptides studied to examine helix disruption and provide model cross sections for comparison to those derived from the ion mobility measurements.

Materials and Methods

Peptide Synthesis. Peptides were synthesized using *FastMoc* (a variant of Fmoc) chemistry with an Applied Biosystems Model 433A peptide synthesizer. After synthesis, the peptides were cleaved from the solid substrate with a 95% trifluoroacetic acid (TFA)/5% water solution, precipitated from solution with cold ethyl ether, washed, and lyophilized. Solutions of 3 mg of peptide in 1 mL of 90% TFA/10% water were electrosprayed. The specific polypeptides studied here include: Ac-A_n (n = 6−20), Ac-A_nGA_m (8−17 residues), Ac-$A_nG_2A_m$ (9−16 residues), Ac-$A_nG_3A_m$ (9−17 residues), Ac-$A_nG_5A_m$ (10−17 residues), Ac-$A_nG_7A_m$ (12−17 residues), Ac-$A_nG_9A_m$ (14−17 residues), and Ac-G_n (n = 7−17). The symmetric peptides (n = m) were synthesized, and ion mobility measurements were performed on the symmetric peptide and the peptide lacking one alanine (the abundance of this byproduct was just sufficient for measurements to be made). The alanine may be deleted from the N-terminus end or the C-terminus end, but there was no indication that these sequence isomers have systematically different structures.

High Resolution Ion Mobility Measurements. The apparatus has been described previously.[12,14,15] Briefly, it consists of an electrospray source, a 63 cm long drift tube, a quadrupole mass spectrometer, and a detector. Ions are electrosprayed in air and enter the drift tube through an "ion gate". The ion gate employs a strong electric field to draw the ions into the drift tube, while a counter flow of helium buffer gas prevents air and solvent molecules from entering. The drift tube is operated with helium buffer gas at slightly above atmospheric pressure and with a drift field of 158.7 V/cm. At the end of the drift tube, some of the ions exit through a small aperture and are then focused into a quadrupole mass spectrometer where they are mass analyzed. The transmitted ions are then detected by an off-axis collision dynode and dual microchannel plates.

10.1021/jp004446d CCC: $20.00 © 2001 American Chemical Society
Published on Web 04/19/2001

Drift times are measured using the depletion mode, where ions are continuously admitted into the drift tube save for short pulses of ~1 ms when the flow of ions is interrupted by an electrostatic shutter in the ion gate. Arrival times, the amount of time it takes for the pulse to travel through the drift tube and reach the detector, are measured using a multichannel scaler synchronized with the electrostatic shutter. Drift time distributions are then obtained by correcting the arrival times for the time the ions spend traveling between the end of the drift tube and the detector. The measured drift times are converted into collision cross sections using[16]

$$\Omega_{\mathrm{avg}}^{(1,1)} = \frac{(18\pi)^{1/2}}{16}\left[\frac{1}{m}+\frac{1}{m_{\mathrm{b}}}\right]^{1/2}\frac{ze}{(k_{\mathrm{B}}T)^{1/2}}\frac{t_{\mathrm{D}}E}{L}\frac{1}{\rho} \qquad (1)$$

where m and m_{b} are the masses of the ion and buffer gas atom, respectively, ze is the ion's charge, ρ is the buffer gas number density, L is the length of the drift tube, and E is the drift field.

Molecular Dynamics Simulations. Molecular dynamics simulations were performed on the 15-residue Ac-$A_nG_xA_n$+H^+ peptides to examine helix disruption by the block of glycines and to determine orientationally averaged cross sections for comparison with the measured values. The MD simulations were performed with the MACSIMUS suite of programs[17] using CHARMM potentials (21.3 parameter set)[18] with a dielectric constant of 1.0. A series of five 300 K 960 ps MD simulations were performed for each 15-residue peptide starting from an α-helical conformation. In addition, a series of "gentle" simulated annealing[19] runs were performed for each peptide starting from both an α-helix and a fully extended, all-trans conformation. The annealing schedule consisted of 100 or 240 ps at 600 K, followed by 240 ps at 500 K, 240 ps at 400 K, and 480 ps at 300 K. A variety of schedules were tried including exponential[19] and logarithmic (simulated quenching)[20] and the linear stepped schedule seemed to provide consistently lower energy structures. At least 30 simulated annealing runs were performed for each peptide starting from an extended all-trans geometry (most of these generated globules), and at least 10 simulated annealing runs were performed for each peptide starting from an α-helix (many of these remained helical, though fewer for the glycine-rich peptides). Average energies, average ϕ and ψ angles, and average collision cross sections were obtained from the final 35 ps of each simulation. Cross sections were calculated using an empirical correction to the exact hard spheres scattering model,[15] averaging over 50 snapshots taken from the final 35 ps of each simulation. If the conformation is correct in the simulation, the calculated cross sections are expected to be within 2% of the measured values.

Since the N-termini of the protonated peptides studied here are acetylated, there is a question about the site of protonation. The quantum chemical calculations of Zhang et al.[21] indicate that the protonation site is probably a backbone carbonyl group (the backbone CO is more basic than a backbone NH). Since protonation near to the C-terminus stabilizes the helical conformation, most of the MD simulations were performed with the backbone carbonyl group nearest the C-terminus protonated. Some simulations were performed with the carbonyl group in the middle of the peptide protonated (residue 8) and some were performed with the carbonyl group nearest the N-terminus protonated.

Results

Cross Section Measurements. Figure 1 shows the relative cross sections for the main features observed in the drift time distributions for Ac-A_n, Ac-A_nGA_m, Ac-$A_nG_3A_m$, Ac-$A_nG_5A_m$, Ac-$A_nG_7A_m$, Ac-$A_nG_9A_m$, and Ac-G_n plotted against the total number of residues. The results for Ac-$A_nG_2A_m$ are similar to those for Ac-A_n and Ac-A_nGA_m, and were not included in the plot for clarity. The relative cross sections plotted in the figure were obtained from $\Omega_{\mathrm{avg}}^{(1,1)} - 14.50(n+m) - 11.86x$, where the measured collision cross section, $\Omega_{\mathrm{avg}}^{(1,1)}$, is in Å^2, $n+m$ is the number of alanine residues in the peptide, x is the number of glycine residues, and 14.50 and 11.86 Å^2 are the increments per residue in the calculated cross sections for ideal ($\phi = -57°$ and $\psi = -47°$) polyalanine and polyglycine α-helices, respectively. Using this scale, the measured relative cross sections for an α-helix are independent of the number of residues, while the relative cross sections for a more compact globule decrease with an increasing number of residues. The results for Ac-A_n+H^+ in Figure 1 are representative of what is expected for a helix, while the results for Ac-G_n+H^+ illustrate the behavior expected for a globule. The dashed line in the figure shows the relative cross sections for (un-acetylated) A_n+H^+ peptides which are also globular.[7]

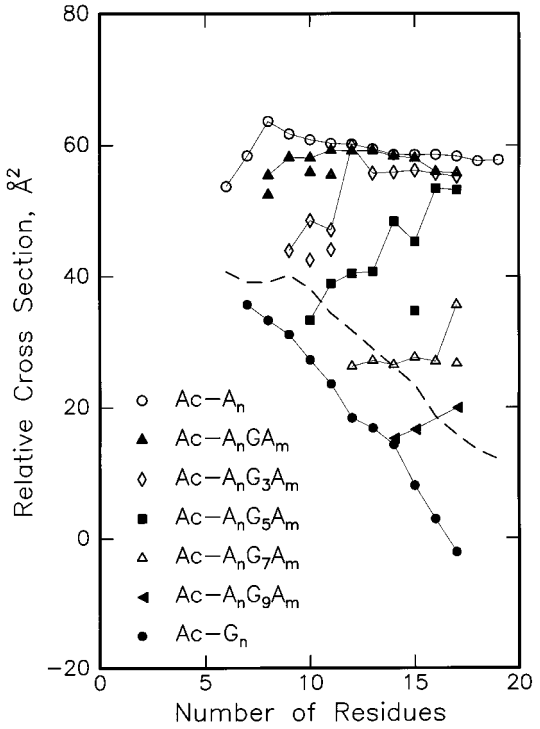

Figure 1. Plot of the measured relative collision cross sections (see text) against the total number of residues. The dashed line shows relative cross sections for A_n+H^+ peptides from ref 7.

The relative cross sections for Ac-$A_nG_xA_m$+H^+ peptides with $x = 1$ and 2 closely track the results for helical Ac-A_n+H^+ (the results for $x = 2$ are not shown in Figure 1). However, as the block of glycines is increased to $x = 3$, deviations begin to emerge. The relative cross sections for peptides with three glycines track those for helical Ac-A_n+H^+ when the total number of residues is ≥ 12. Ac-$A_nG_3A_m$+H^+ peptides with <12 residues have significantly smaller relative cross sections than the helical Ac-A_n+H^+. For peptides with a block of five glycines the deviations are even more evident. The smaller Ac-$A_nG_5A_m$+H^+ peptides have relative cross sections close to those for the globular Ac-G_n+H^+. As the number of residues increases, the relative cross sections increase and for ≥ 16 residues, the relative cross sections are close to the values for helical Ac-A_n+H^+. Thus the critical number of residues for helix formation in Ac-$A_nG_5A_m$+H^+ peptides is 16, compared to 12

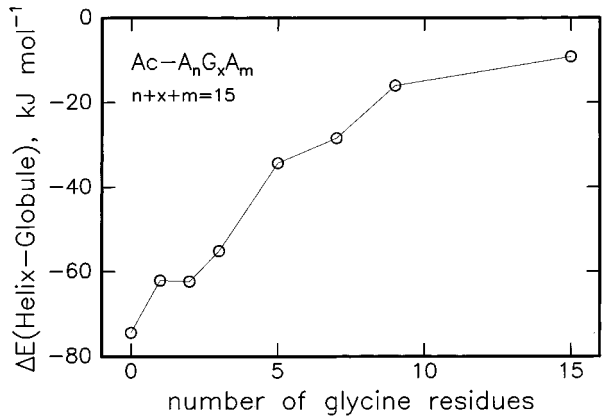

Figure 2. Plot of the calculated energy difference between the lowest energy helical conformation and the lowest energy globule against the number of glycine residues for various 15-residue polypeptides.

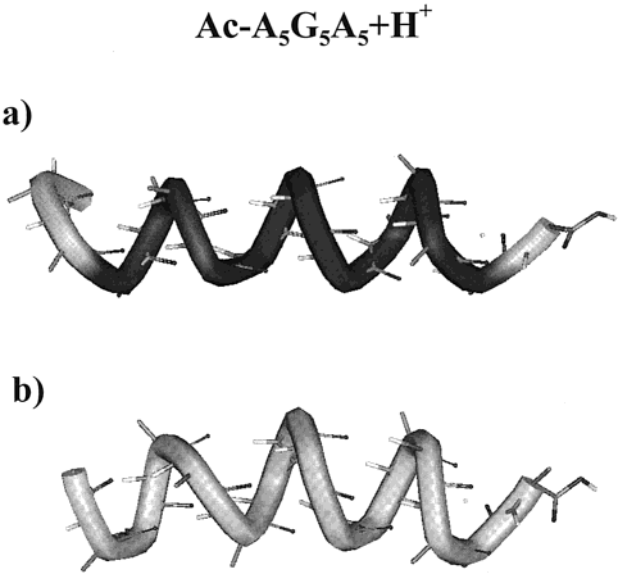

Figure 3. The different types of helices found for Ac-$A_5G_5A_5$+H^+ in the simulations: (a) α-helix and (b) α/π-helix.

in the Ac-$A_nG_3A_m$+H^+ peptides. The relative cross sections for Ac-$A_nG_7A_m$+H^+ and Ac-$A_nG_9A_m$+H^+ peptides are all substantially smaller than those for the helical Ac-A_n+H^+ in the size range examined (up to 17 residues). For several peptides (Ac-A_nGA_m+H^+ with 8, 10, and 11 residues; Ac-$A_nG_3A_m$+H^+ with 10 and 11 residues; Ac-$A_nG_5A_m$+H^+ with 15 residues; and Ac-$A_nG_7A_m$+H^+ with 17 residues) more than one conformation was resolved in the drift time distributions (see Figure 1).

Molecular Dynamics Simulations. The energy differences between lowest energy helical structures and the lowest energy globule found in the simulations are plotted in Figure 2. The energy difference declines as the number of glycine residues increases. For peptides with <7 glycine residues, the average ϕ and ψ angles for the lowest energy helices (except for the first one or two residues at both ends) are within a degree of the ideal values for an α-helix ($\phi = -57°$ and $\psi = -47°$). For peptides with ≥7 glycines, the average ϕ and ψ angles for the lowest energy helices (ignoring the ones at the ends) are ∼61° and ∼58°, respectively. These are between the values expected for an α-helix ($\phi = -57°$ and $\psi = -47°$) and a π-helix ($\phi = -57°$ and $\psi = -70°$). We will refer to this as an α/π-helix. Both α-helices and α/π-helices were found for peptides with 3, 5, and 7 glycines. The lowest energy α-helix and α/π-helix found for Ac-$A_5G_5A_5$+H^+ are shown in Figure 3.

The average energies and cross sections for the lowest energy α-helix, α/π-helix, and globule are shown in Table 1. Calculated cross sections for the lowest energy α-helices agree with the measured values (to within 2%) for peptides with ≤3 glycines (see Table 1). For peptides with >3 glycines, the measured cross sections are no longer close to those calculated for an α-helix. For Ac-$A_5G_5A_5$+H^+, the α/π-helix has a calculated cross section that is within 1% of the larger of the two cross sections measured for this peptide. According to our simulations, the α/π-helix is almost degenerate with the α-helix for Ac-$A_5G_5A_5$+H^+. The smaller cross section measured for this peptide falls between the calculated values for the α/π-helix and the globule. The measured cross section for Ac-$A_4G_7A_4$+H^+ also falls between the values calculated for the α/π-helix and the globule. It is not clear whether these intermediate values result from a stable conformation with a geometry between the helix and globule, or from rapid interconversion between the helix and globule. If interconversion is rapid on the time scale of the measurements (which is ∼100 ms), then a single peak with a drift time corresponding to the time averaged cross section is obtained.

The cross section calculated for the lowest energy globule for Ac-$A_3G_9A_3$+H^+ is 2% larger than the measured value. For Ac-G_{15}+H^+ the deviation is much larger. The cross section calculated for the lowest energy globule is 9% larger than the measured cross section. More compact conformations with cross sections that come closer to the measured value were found.

The most compact conformation found in these simulations had a cross section of 187 Å^2 (which is very close to the measured value). This conformations was ∼15 kJ mol^{-1} higher in energy than the lowest energy Ac-G_{15}+H^+ globule shown in Table 1. The discrepancy between the measured and calculated cross sections for Ac-G_{15}+H^+ probably occurs because of the difficulty in finding compact low-energy globules through MD simulations. If we were to run more or longer MD simulations we would eventually find more-compact and lower energy conformations. We are currently developing more advanced methods to seek out these conformations.

In the simulations described above it was assumed that the protonation site was the backbone carbonyl group nearest to the C-terminus. While this is a reasonable assumption for the helices, the proton may migrate to another site in the globules if this leads to a lower energy conformation. To examine this issue, MD simulations were performed with peptides protonated at the backbone carbonyl on residue 8 (the midpoint) and on residue 1 (the N-terminus). For Ac-G_{15}+H^+ protonated at the N-terminus, the lowest energy globule was within 3 kJ mol^{-1} of the lowest energy globule protonated at the C-terminus. However, the cross section for lowest energy globule protonated at the N-terminus (186 Å^2) agrees with the measured value, unlike the one protonated at the C-terminus (see Table 1). The lowest energy globule for Ac-G_{15}+H^+ protonated at the midpoint was slightly higher in energy and slightly less compact. For Ac-$A_4G_7A_4$+H^+ protonated at the midpoint, the lowest energy globule was 9 kJ mol^{-1} lower than the lowest energy globule protonated at the C-terminus. The cross section for the globule protonated at the midpoint (226 Å^2) agrees with the measured value (see Table 1). These results suggest that the alternate protonation sites may lead to slightly lower energy globular conformations.

TABLE 1: Comparison of Measured and Calculated Cross Sections for Ac-$A_nG_xA_m$ Peptides: Average Energies and Cross Sections from the Lowest Energy α-Helix, α/π-Helix, and Globule Simulations Shown

		α-helix		α/π-helix		globule	
peptide	measured cross section, Å^2	energy, kJ mol^{-1}	cross section, Å^2	energy, kJ mol^{-1}	cross section, Å^2	energy, kJ mol^{-1}	cross section, Å^2
Ac-A_{15}	276	−2876	278			−2802	247
Ac-A_7GA_7	273	−2874	277			−2812	241
Ac-$A_6G_2A_7$	269	−2872	273			−2810	238
Ac-$A_6G_3A_6$	265	−2871	271	−2863	258	−2816	240
Ac-$A_5G_5A_5$	249, 239	−2868	264	−2866	251	−2833	225
Ac-$A_4G_7A_4$	227	−2865	258	−2875	244	−2846	217
Ac-$A_3G_9A_3$	210			−2876	238	−2860	215
Ac-G_{15}	186			−2900	213	−2890	203

Discussion

In previous work, polyalanine peptides were shown to adopt a helical conformation when protonated at a C-terminus lysine.[10] In these helical Ac-A_nK+H^+ peptides, protonation at the N-terminus is blocked by acetylation, and the lysine side chain is the most basic site. The observation that Ac-A_n+H^+ peptides are helical indicates that the C-terminus lysine is not necessary to direct helix formation, simply blocking the basic N-terminus is sufficient. With the N-terminus blocked, and with no basic side chains, protonation must occur on the backbone amide groups. But where? For the helices, protonation near the C-terminus is expected since this will stabilize the helical conformation. For the globule, protonation anywhere along the backbone is feasible.

Glycine disrupts helix formations in aqueous solution and in unsolvated peptides. Helix disruption by glycine in aqueous solution may be partly due to the absence of a side chain allowing solvent access to the polar groups along the helix backbone.[22] However, glycine's low helix propensity in solution is usually attributed mainly to backbone entropy.[23] With no side-chain, glycine can sample more conformational space than the other amino acids, so the entropy cost of helix formation is larger. Some calculations suggest that in the gas phase the entropic penalty for helix formation with glycine is actually slightly *less* than for amino acids with side chains.[24] So backbone entropy may not be responsible for glycine's low helix propensity in the gas phase. In the results of our MD simulations, the average energy difference between the helix and globule decreases as the number of glycine residues increases (see Figure 2). These energy differences can be considered to approximate the enthalpy differences. The reason that the enthalpy difference decreases as the number of glycine residues increases probably has nothing to do with the stability of the helix itself, it is probably due to the stability of the globule. Because of glycine's small size and extra conformational freedom, glycine-rich peptides are able to pack into more compact and lower energy globules than alanine-rich peptides.[11]

According to the measured relative cross sections the helical conformation appears to breakdown for 15-residue peptides when a block of five glycines is incorporated. On the other hand, according to the simulations, the helix is the energetically favored conformation even for Ac-G_{15}+H^+ (see Figure 2). There are several plausible explanations for this discrepancy between the simulations and experiment. The energy (enthalpy) differences shown in Figure 2 ignore the entropic contributions to the free energy. As noted above, entropy is expected to favor the globule. If this is the case, the free energy differences between the helix and globule will all be more positive than the enthalpies shown in Figure 2. Another plausible explanation for the discrepancy between the simulations and experiment is that the simulations have not found the lowest energy globules.

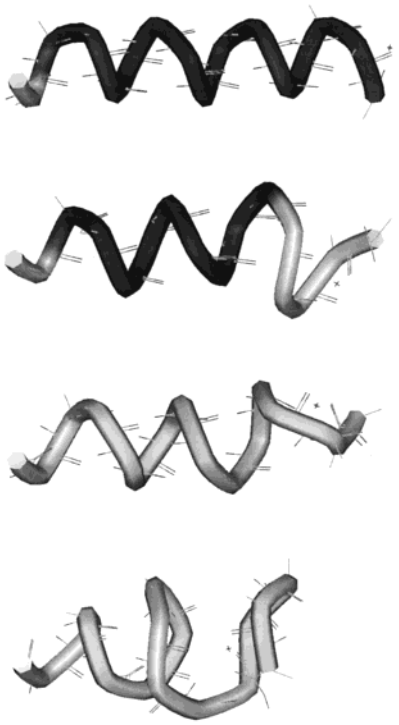

Figure 4. The unfolding of an Ac-$A_3G_9A_3$ helix. Snapshots were taken from the 600 K portion of a simulated annealing run at 0.0, 3.5, 15.4, and 19.6 ps, top to bottom, respectively. The unfolding proceeds from the C-terminus.

This issue was mentioned above in connection with the discrepancy between the measured and calculated cross sections for AcG_{15}+H^+. Simulated annealing is known to have limitations in finding global energy minima.[20,25] In the present case, the low energy globular conformations are expected to be quite compact, and not easily found by simulated annealing. Finally, the classical force field employed in the simulations may not provide a correct evaluation of the energy differences between the helix and globule conformations. The force field employed here, CHARMM, is a relatively simple one, incorporating electrostatic, Lennard-Jones, and internal bonding terms. It is not polarizable[26] and does not account for environment effects.[27] It also does not account for some weak interactions, like for example the C^{α}−H···O═C hydrogen bond.[28]

Helices are usually thought to unravel mainly from their ends, and this is a view that is supported by a number of MD simulations.[29−32] In the Ac-$A_nG_xA_m$+H^+ peptides studied here, the glycine residues are located in the middle while the alanine residues are at the ends. So when the glycine residues disrupt the Ac-$A_nG_xA_m$+H^+ peptides, do they unravel from the ends or from the middle? In the simulations it appears that the disruption originates at the ends. Figure 4 shows a series of

snapshots taken (at 0.0, 3.5, 15.4, and 19.6 ps) during the unfolding of an Ac-$A_3G_9A_3$ helix in the 600 K portion of a simulated annealing run. The unfolding proceeds from the C-terminus where it involves both alanine and glycine residues. One of the factors driving unfolding from the C-terminus is the generation of a structure that more effectively solvates the charge. However, the helices also unravel from the N-terminus. The fact that the peptide does not unravel from the inside supports the idea that the glycines destabilize the helix through a global effect on the relative energies of the helix and globule rather than through a localized entropic effect resulting from glycine's conformational freedom.

Conclusions

We have studied how glycine destabilizes helices by examining Ac-$A_nG_xA_m$+H^+ peptides by high-resolution ion mobility measurements and molecular dynamics simulations. The number of glycines needed to disrupt helix formation scales with the number of residues. More than three glycines are required to disrupt helix formation in a fifteen residue peptide. In the simulations, the energy (enthalpy) difference between the helix and globule steadily decreases as the size of the block of glycines increases. This decrease is attributed to the glycines promoting the formation of lower energy globules (making the energy gap between the helix and globule smaller). The glycines do not cause a localized disruption in the middle of the helices. Instead, the helices appear to unravel from their ends. This suggests that the disruption occurs through a global effect on the relative energies of the helix and globule rather than through a localized entropic effect.

Acknowledgment. We thank Jiri Kolafa for the use of his MACSIMUS molecular modeling programs. We gratefully acknowledge the support of the National Institutes of Health.

References and Notes

(1) For some examples of studies of unsolvated peptides and proteins, see: Suckau, D., Shi, Y.; Beu, S. C.; Senko, M. W.; Quinn, J. P.; Wampler, F. M.; McLafferty, F. W. *Proc. Nat. Acad. Sci. U.S.A.* **1993**, *90*, 790−793. Campbell, S.; Rodgers, M. T.; Marzluff, E. M.; Beauchamp, J. L. *J. Am. Chem. Soc.* **1995**, *117*, 12840−12854. Schnier, P. D.; Price, W. D.; Jockusch, R. A.; Williams, E. R. *J. Am. Chem. Soc.* **1996**, *118*, 7178−7189. Kaltashov, I. A.; Fenselau, C. *Proteins*: *Struct. Funct. Genet.* **1997**, *27*, 165−170. Valentine, S. J.; Clemmer, D. E. *J. Am. Chem. Soc.* **1997**, *119*, 3558−3566. Wyttenbach, T., Bushnell, J. E.; Bowers, M. T. *J. Am. Chem. Soc.* **1998**, *120*, 5098−5103. Arteca, G. A.; Velázquez, I.; Reimann, C. T.; Tapia, O. *Phys. Rev. E* **1999**, *59*, 5981−5986. Schaaff, T. G.; Stephenson, J. L.; McLuckey, S. L. *J. Am. Chem. Soc.* **1999**, *121*, 8907−8919.

(2) Chakrabartty, A.; Baldwin, R. L. *Adv. Protein. Chem.* **1995**, *46*, 141−176.

(3) Marqusee, S., Robbins, V. H., Baldwin, R. L. *Proc. Nat. Acad. Sci. U.S.A.* **1989**, *86*, 5286−5290.

(4) O'Neil, K. T.; DeGrado, W. F. *Science* **1990**, *250*, 646−651.

(5) Padmanabhan, S.; Marqusee, S.; Ridgeway, T.; Laue, T. M.; Baldwin, R. L. *Nature* **1990**, *344*, 268−270.

(6) Lyu, P. C.; Liff, M. I.; Marky, L. A.; Kallenbach, N. R. *Science* **1990**, *250*, 669−673.

(7) Hudgins, R. R.; Mao, Y.; Ratner, M. A.; Jarrold, M. F. *Biophys. J.* **1999**, *76*, 1591−1597.

(8) Zhang, K.; Cassady, C. J.; Chung-Phillips, A. *J. Am. Chem. Soc.* **1994**, *116*, 11512−11521.

(9) Hol, W. G. J.; van Duijnen, P. T.; Berendsen, H. J. C. *Nature* (*London*) **1978**, *273*, 443.

(10) Hudgins, R. R.; Jarrold, M. F. *J. Am. Chem. Soc.* **1999**, *121*, 3494−3501.

(11) Hudgins, R. R.; Jarrold, M. F. *J. Phys. Chem. B* **2000**, *104*, 2154−2158.

(12) Dugourd, P.; Hudgins, R. R.; Clemmer, D. E.; Jarrold, M. F. *Rev. Sci. Instrum.* **1997**, *68*, 1122−1129.

(13) Hudgins, R. R.; Ratner, M. A.; Jarrold, M. F. *J. Am Chem. Soc.* **1998**, *120*, 12974−12975.

(14) Hudgins, R. R., Woenckhaus, J.; Jarrold, M. F. *Int. J. Mass. Spectrom. Ion. Proc.* **1997**, *165/166*, 497−507.

(15) Kinnear, B. S.; Kaleta, D. T.; Kohtani, M.; Hudgins, R. R.; Jarrold, M. F. *J. Am. Chem. Soc.* **2000**, *122*, 9243−9256.

(16) Mason, E. A.; McDaniel, E. W. *Transport Properties of Ions in Gases*; Wiley: New York, 1988.

(17) http://www/icpf.cas.cz/jiri/macsimus/default.htm.

(18) Brooks, B. R.; Bruccoleri, R. E.; Olafson, B. D.; States, D. J.; Swaminathan, S.; Karplus, M. *J. Comput. Chem.* **1983**, *4*, 187−217.

(19) Kirkpatrick, S.; Gelatt, Jr., C. D.; Vecchi, M. P. *Science* **1983**, *220*, 671−680.

(20) Ingber, L. *Math. Comput. Modell.* **1993**, *18*, 29−57.

(21) Zhang, K.; Cassady, C. J.; Chung-Phillips, A. 1994. *J. Am. Chem. Soc.* **1994**, *116*, 11512−11521.

(22) Luo, P.; Baldwin, R. L. *Proc. Nat. Acad. Sci. U.S.A.* **1999**, *96*, 4930−4935.

(23) Gō, M.; Gō, N.; Scheraga, H. *J. Chem. Phys.* **1970**, *52*, 2060−2079.

(24) Okamoto, Y.; Hansmann, U. H. E. *J. Phys. Chem.* **1995**, *99*, 11276−11287.

(25) Nayeem, A.; Vila, J.; Scheraga, H. A. *J. Comput. Chem.* **1991**, *12*, 594−605.

(26) Banks, J. L.; Kaminski, G. A.; Zhou, R. H.; Mainz, D. T.; Berne, B. J.; Friesner, R. A. *J. Chem. Phys.* **1999**, *110*, 741−754.

(27) Rick, S. W.; Cachau, R. E. *J. Chem. Phys.* **2000**, *112*, 5230−5241.

(28) Vargas, R.; Garza, J.; Dixon, D. A.; Hay, B. P *J. Am. Chem. Soc.* **2000**, *122*, 4750−4755.

(29) Tirado-Rives, J.; Jorgensen, W. L. *Biochem.* **1991**, *30*, 3864−3871.

(30) Daggett, V.; Kollman, P. A.; Kuntz, I. D. *Biopolymers* **1991**, *31*, 1115−1134.

(31) Daggett, V.; Levitt, M. *J. Mol. Biol.* **1992**, *223*, 1121−1138.

(32) Samuelson, S.; Martyna, G. J. *J. Phys. Chem. B* **1999**, *103*, 1752−1766.